0026-895X/11/8006-1096–1107$25.00
MOLECULAR PHARMACOLOGY
Vol. 80, No. 6
73833/3734151
Mol Pharmacol 80:1096–1107, 2011
Printed in U.S.A.

Therapeutic Targeting of a Novel 6-Substituted Pyrrolo [2,3-*d*]pyrimidine Thienoyl Antifolate to Human Solid Tumors Based on Selective Uptake by the Proton-Coupled Folate Transporter[S]

Sita Kugel Desmoulin, Lei Wang, Eric Hales, Lisa Polin, Kathryn White, Juiwanna Kushner, Mark Stout, Zhanjun Hou, Christina Cherian, Aleem Gangjee, and Larry H. Matherly

Graduate Program in Cancer Biology (S.K.D., L.H.M.), Departments of Oncology (S.K.D., L.P., E.H., Z.H., C.C., L.H.M.) and Pharmacology (L.H.M.), and Division of Hematology-Oncology, Department of Internal Medicine (K.W., J.K.), Wayne State University School of Medicine, Detroit, Michigan; Department of Pediatrics, Children's Hospital of Michigan, Detroit, Michigan (M.S.); Developmental Therapeutics Program, Barbara Ann Karmanos Cancer Institute, Detroit, Michigan (L.P., E.H., Z.H., C.C., L.H.M.); and Division of Medicinal Chemistry, Graduate School of Pharmaceutical Science, Duquesne University, Pittsburgh, Pennsylvania (L.W., A.G.)

Received May 27, 2011; accepted September 22, 2011

ABSTRACT

The proton-coupled folate transporter (PCFT) is a proton-folate symporter with an acidic pH optimum. By real-time reverse transcription-polymerase chain reaction, PCFT was expressed in the majority of 53 human tumor cell lines, with the highest levels in Caco-2 (colorectal adenocarcinoma), SKOV3 (ovarian), and HepG2 (hepatoma) cells. A novel 6-substituted pyrrolo[2,3-*d*]pyrimidine thienoyl antifolate (compound **1**) was used to establish whether PCFT can deliver cytotoxic drug under pH conditions that mimic the tumor microenvironment. Both **1** and pemetrexed (Pmx) inhibited proliferation of R1-11-PCFT4 HeLa cells engineered to express PCFT without the reduced folate carrier (RFC) and of HepG2 cells expressing both PCFT and RFC. Unlike Pmx, **1** did not inhibit proliferation of R1-11-RFC6 HeLa cells, which express RFC without PCFT. Treatment of R1-11-PCFT4 cells at pH 6.8 with **1** or Pmx inhibited colony formation with dose and time dependence. Transport of [^{3}H]compound **1** into R1-11-PCFT4 and HepG2 cells was optimal at pH 5.5 but appreciable at pH 6.8. At pH 6.8, [^{3}H]compound **1** was metabolized to ^{3}H-labeled polyglutamates. Glycinamide ribonucleotide formyltransferase (GARFTase) in R1-11-PCFT4 cells was inhibited by **1** at pH 6.8, as measured by an in situ GARFTase assay, and was accompanied by substantially reduced ATP levels. Compound **1** caused S-phase accumulation and a modest level of apoptosis. An in vivo efficacy trial with severe combined immunodeficient mice implanted with subcutaneous HepG2 tumors showed that compound **1** was active. Our findings suggest exciting new therapeutic possibilities to selectively deliver novel antifolate drugs via transport by PCFT over RFC by exploiting the acidic tumor microenvironment.

Introduction

Antifolates are some of the most versatile and best understood cancer chemotherapy drugs. These agents, notably aminopterin, revolutionized the treatment of acute lymphoblastic leukemia by inducing complete remissions in children with leukemia (Farber and Diamond, 1948). Aminopterin and methotrexate (Mtx) were recognized to disrupt folate metabolism by inhibiting dihydrofolate reductase (Monahan and Allegra, 2006). Subsequent generations of antifolates

This study was supported by the National Institutes of Health National Cancer Institute [Grants CA53535, CA152316, CA125153]; the Barbara Ann Karmanos Cancer Institute; the Mesothelioma Applied Research Foundation; and a Doctoral Research Award from the Canadian Institutes of Health Research (to S.K.D.).

L.H.M. and A.G. contributed equally to this work.

Article, publication date, and citation information can be found at http://molpharm.aspetjournals.org.

doi:10.1124/mol.111.073833.

[S] The online version of this article (available at http://molpharm.aspetjournals.org) contains supplemental material.

ABBREVIATIONS: Mtx, methotrexate; Pmx, pemetrexed; GAR, β-glycinamide ribonucleotide; GARFTase, β-glycinamide ribonucleotide formyltransferase; RFC, reduced folate carrier; FR, folate receptor; PCFT, proton-coupled folate transporter; h, human; LCV, leucovorin; RT-PCR, reverse transcription-polymerase chain reaction; GAPDH, glyceraldehyde-3-phosphate dehydrogenase; dFBS, dialyzed fetal bovine serum; DMSO, dimethyl sulfoxide; PIPES, 25 mM piperazine-*N*,*N*′-bis(2-ethanesulfonic acid; DPBS, Dulbecco's phosphate-buffered saline; MES, 2-(*N*-morpholino)ethanesulfonic acid; HPLC, high-performance liquid chromatography; FITC, fluorescein isothiocyanate; PI, propidium iodide; SCID, severe combined immunodeficiency; ALL, acute lymphoblastic leukemia; CHO, Chinese hamster ovary; MTAP, methylthioadenosine phosphorylase.

primarily targeted other key folate-dependent enzymes, including thymidylate synthase [pemetrexed (Pmx)] and β-glycinamide ribonucleotide (GAR) formyltransferase (GARFTase) (lometrexol). For all these agents, cellular uptake and metabolism to polyglutamates are critical to drug activity (Mendelsohn et al., 1999; Monahan and Allegra, 2006; Chattopadhyay et al., 2007).

The anionic nature of antifolates precludes their diffusion across biological membranes. Three genetically distinct and functionally diverse transport systems have evolved to facilitate their uptake into mammalian cells. 1) The reduced folate carrier (RFC; SLC19A1), a member of the major facilitator superfamily of solute carriers, is an anionic antiporter and the major transport system for reduced folates in mammalian cells and tissues at physiologic pH (Matherly et al., 2007). RFC is ubiquitously expressed in normal and malignant tissues. 2) Folate receptors (FRs) α and β are glycosylphosphatidylinositol-anchored membrane proteins that transport folates by receptor-mediated endocytosis. FRα is expressed in epithelial cells of the kidney, choroid plexus, retina, uterus, and placenta. Malignant tissues also express FRα, including adenocarcinomas of the cervix, uterus, and ovary (Elnakat and Ratnam, 2004). 3) The proton-coupled folate transporter (PCFT; SLC46A1) is a proton-folate symporter that functions optimally at acidic pH by coupling the downhill flow of protons to the uphill flow of folates into cells (Qiu et al., 2006; Nakai et al., 2007; Zhao and Goldman, 2007). PCFT is expressed in normal mouse and human tissues. High PCFT levels are present at the apical brush-border membrane along the proximal jejunum and duodenum, and in kidney, liver, placenta, and choroid plexus, whereas much lower levels were detected in other tissues (Qiu et al., 2007; Zhao et al., 2009; Kugel Desmoulin et al., 2010a). Although a low pH transport activity was described in human tumor cell lines of assorted origins (Zhao et al., 2004), presumably as a result of PCFT, tumor expression of PCFT has not been systematically studied.

There is now ample precedent for using FRα to selectively target tumors with cytotoxic agents for therapeutic benefit (Gibbs et al., 2005; Hilgenbrink and Low, 2005; Salazar and Ratnam, 2007; Deng et al., 2008, 2009; Wang et al., 2010). PCFT transport function may be enhanced in many solid tumors by the acidic pH of the tumor microenvironment, which has been reported to reach as low as pH 6.2 to 6.8 (Wike-Hooley et al., 1984; Helmlinger et al., 1997; Raghunand et al., 1999). Intracellular pH is normally alkaline, which creates a substantial transmembrane pH gradient directed *intra*cellularly (Fais et al., 2007). Clearly, harnessing this proton-motive gradient to transport cytotoxic antifolates into tumor cells by PCFT offers a uniquely attractive mechanism of therapeutic targeting solid tumors.

For tumor targeting of cytotoxic drugs via FR or PCFT, ideally, therapeutic agents have been developed that are specifically transported by FRs and/or PCFT and not by RFC (Gibbs et al., 2005; Hilgenbrink and Low, 2005; Salazar and Ratnam, 2007; Deng et al., 2008, 2009; Kugel Desmoulin et al., 2010b; Wang et al., 2010). This strategy is necessary because antifolate membrane transport by RFC precludes tumor selectivity, in that RFC is expressed in both normal and tumor cells, and RFC transport is optimal at neutral pH characterizing most normal tissues (Zhao and Goldman, 2003; Matherly et al., 2007). Indeed, a major obstacle in implementing this approach has been a lack of FR- or PCFT-selective antifolates, because all of the clinically useful antifolates with significant FR- and PCFT substrate activity (e.g., Mtx and Pmx) are also transported by RFC (Matherly et al., 2007).

We recently described a novel 2-amino-4-oxo-6-substituted pyrrolo[2,3-*d*]pyrimidine antifolate with a thienoyl-for-benzoyl replacement and a bridge length of four carbons (compound **1**) (Fig. 1) (Wang et al., 2010). Cellular uptake of compound **1** by FRα was substantial in the absence of its membrane transport by RFC, resulting in potent antitumor activity both in vitro and in vivo because of inhibition of GARFTase in de novo purine nucleotide biosynthesis. Although transport of compound **1** by PCFT was also inferred, neither this nor the capacity of PCFT to deliver a cytotoxic dose of compound **1** under conditions relevant to the solid tumor microenvironment was directly tested.

This report describes such experiments with compound **1** to establish the feasibility of selectively targeting chemotherapy to human solid tumors based upon drug membrane transport by PCFT. Experiments are also described documenting the PCFT transport and polyglutamylation characteristics of compound **1**, which account for its potent inhibition of GARFTase leading to tumor cell death in vitro and in vivo.

Materials and Methods

Materials. [3′,5′,7-^{3}H]Mtx (20 Ci/mmol), [^{3}H]Pmx (2.5 Ci/mmol), and custom-radiolabeled [^{3}H]compound **1** (1.3 Ci/mmol) were purchased from Moravek Biochemicals (Brea, CA). Leucovorin (LCV) [(6*R*,*S*)-5-formyl tetrahydrofolate] was provided by the Drug Development Branch, National Cancer Institute (Bethesda, MD). Pmx [*N*-{4-[2-(2-amino-3,4-dihydro-4-oxo-7H-pyrrolo[2,3-d]pyrimidin-5-yl)ethyl] benzoyl}-L-glutamic acid] (Alimta) was provided by Eli Lilly and Co. (Indianapolis, IN). Synthesis and properties of the substituted pyrrolo[2,3-*d*]pyrimidine antifolate compound **1** were described previously (Wang et al., 2010). Other chemicals were obtained from commercial sources in the highest available purities.

Cell llines. The sources and cell culture conditions for the panel of human solid tumor and leukemia cell lines used for quantitative RT-PCR assays of transcript levels for FRα, hPCFT, and hRFC are summarized in Supplemental Table 1S. HeLa R1-11-RFC6 and R1-11-PCFT4 cells were derived from human RFC (hRFC)- and human PCFT (hPCFT)-null R1-11 cells by stable transfection with HA-tagged pZeoSV2(+)-RFC and pZeoSV2(+)-PCFT constructs, respectively (Zhao et al., 2008). These HeLa sublines, along with R1-11-mock transfected cells, were gifts from Dr. I. David Goldman (Albert Einstein School of Medicine, Bronx, NY). Characteristics and maintenance of the HeLa sublines were described previously (Zhao et al., 2008).

Real-Time RT-PCR Analysis of RFC, FRα, and PCFT Transcripts. RNAs were isolated from a variety of human cell lines, including solid tumor (n = 53) and leukemia (n = 27) sublines (Supplemental Table 1S) and engineered R1-11 HeLa sublines (R1-11 mock, R1-11-RFC6, and R1-11-PCFT4), using TRIzol reagent

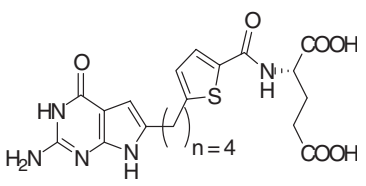

Fig. 1. Structure of 6-substituted pyrrolo[2,3-*d*]pyrimidine thienoyl antifolate compound (Wang et al., 2010).

(Invitrogen, Carlsbad, CA). cDNAs were synthesized using SuperScript reverse transcriptase III kit (Invitrogen). cDNAs were purified with the QIAquick PCR Purification Kit (QIAGEN, Valencia, CA). Quantitative real-time RT-PCR was performed on a Roche LightCycler 480 using Universal Probes (Roche, Indianapolis, IN) and gene-specific primers. Primers are included in Supplemental Table 2S. Transcript levels for FRα, hPCFT, and hRFC genes were normalized to those for glyceraldehyde-3-phosphate dehydrogenase (GAPDH) using commercial probes and primers (Universal ProbeLibrary Human GAPD Gene Assay; Roche Applied Science, Indianapolis, IN). External standard curves were constructed for each gene of interest using serial dilutions of linearized templates, prepared by amplification from suitable cDNA templates, subcloning into a TA-cloning vector (PCR-Topo; Invitrogen), and restriction digestions.

Proliferation and Colony-Forming Assays. For growth inhibition assays, R1-11-PCFT4, R1-11-RFC6 HeLa, and HepG2 cells were cultured in folate-free RPMI 1640 medium, pH 7.2, containing 25 nM LCV, supplemented with 10% dialyzed fetal bovine serum (dFBS; Invitrogen), 2 mM L-glutamine, 100 units/ml penicillin, and 100 μg/ml streptomycin for at least 2 weeks. Cells were plated in 96-well culture dishes (5000 cells/well; 200 μl/well) in the above medium with a broad concentration range of drugs (depending on the compound, drug dilutions were in DMSO or water with appropriate vehicle controls); cells were incubated for up to 96 h at 37°C in a CO_2 incubator. Metabolically active cells (a measure of cell viability) were assayed with CellTiter-Blue cell viability assay (Promega, Madison, WI) and a fluorescent plate reader (emission at 590 nm, excitation at 560 nm) for determining IC_{50} values, corresponding to drug concentrations that result in 50% loss of cell growth.

For colony-forming assays, folate-depleted R1-11-PCFT4 cells (500 cells) in log-phase were plated into 60-mm dishes in folate-free RPMI 1640 medium, supplemented with 25 nM LCV, 10% dFBS, penicillin-streptomycin, and 2 mM L-glutamine, pH 7.2, and allowed to adhere for 48 h. Cells were then treated with compound **1** or Pmx in the above media, supplemented with 25 mM PIPES and 25 mM HEPES to maintain the pH at 6.8. After 16, 24, or 48 h, cells were rinsed with Dulbecco's phosphate-buffered saline (DPBS), then incubated in drug-free, complete folate-free RPMI 1640 medium plus dFBS, supplemented with 25 nM LCV, pH 7.2. Cells were allowed to outgrow for 12 days, at which time the dishes were rinsed with DPBS, 5% trichloroacetic acid, and borate buffer (10 mM, pH 8.8), followed by 1% methylene blue (in borate buffer). The dishes were again rinsed with borate buffer, and colonies were counted for calculating percentage colony formation relative to the DMSO controls.

Transport Assays. To determine the pH-dependent transport of [^{3}H]compound **1** and [^{3}H]Pmx (both at 0.25 μM) in R1-11-PCFT4, R1-11-mock, and HepG2 cells, uptake was assayed at 37°C in cell monolayers over 2 to 30 min at 37°C in complete folate-free RPMI 1640 (pH 5.5, 6.8, and 7.2), supplemented with 10% dFBS and 25 mM HEPES/25 mM PIPES. At the end of the incubations, transport was quenched with ice-cold DPBS, cells were washed three times with ice-cold DPBS, and cellular proteins were solubilized with 0.5 N NaOH. Levels of drug uptake were expressed as picomoles per milligram of protein, calculated from direct measurements of radioactivity and protein contents of cell homogenates. Proteins were quantified using Folin-phenol reagent (Lowry et al., 1951).

For PCFT transport kinetic analyses, R1-11-PCFT4 cells were grown in suspension using spinner flasks at densities of 2 to 5×10^5 cells/ml. Cells were collected by centrifugation, washed with DPBS, and suspended (at 1.5×10^7 cells) in 2 ml of transport buffer (below) for cellular uptake assays. To determine [^{3}H]compound **1** and [^{3}H]Pmx kinetic constants for PCFT (K_t and V_{max}), initial uptake rates were measured at 37°C over 2 min in HEPES-buffered saline (20 mM HEPES, 140 mM NaCl, 5 mM KCl, 2 mM $MgCl_2$, and 5 mM glucose) at pH 6.8, or in MES-buffered saline (20 mM MES, 140 mM NaCl, 5 mM KCl, 2 mM $MgCl_2$, and 5 mM glucose) at pH 5.5 (Zhao et al., 2004), using substrate concentrations from 0.04 to 5 μM. K_t and V_{max} values were determined from Lineweaver-Burk plots.

HPLC Analysis of Polyglutamyl Derivatives of Compound 1 and Pmx. Folate-depleted R1-11-PCFT4 and HepG2 cells were grown in complete folate-free RPMI 1640 medium, supplemented with 25 nM LCV and 10% dFBS. Cells were washed with DPBS and incubated in complete RPMI 1640 medium with dFBS and 25 mM PIPES/25 mM HEPES, pH 6.8, with 1 μM [^{3}H]compound **1** or [^{3}H]Pmx at 37°C in the presence of 60 μM adenosine, or 60 μM adenosine plus 10 μM thymidine, respectively. After 16 h, cells were washed three times with ice-cold DPBS, then scraped mechanically into 5 ml of ice-cold DPBS, pelleted, and flash-frozen. The cell pellets were resuspended into 0.5 ml of 50 mM sodium phosphate buffer, pH 6, and 100 mM 2-mercaptoethanol, including unlabeled compound **1** (or Pmx) and Mtx-diglutamate, -triglutamate, and -tetraglutamate standards (Schircks Laboratories, Jona, Switzerland) (50 μM each). A portion (50 μl) was used to determine total [^{3}H]compound **1** or Pmx (in picomoles per milligram of protein). Proteins were measured by the Bio-Rad protein assay (Bio-Rad Laboratories, Richmond, CA). The remaining extract was boiled (10 min), the supernatant containing radiolabeled compound **1** (or Pmx) and its metabolites was centrifuged, then (250 μl) injected into a Waters 4 μm Nova-Pak C-18 column (3.9 $\times$ 150 mm) with a Nova-Pak 4 μm C-18 guard column. A Varian 9012 ternary gradient-programmable pump was used for gradient development, and a 9050 Varian UV/Vis detector set to 313 nm was used for detection of compound **1**, Pmx, or Mtx polyglutamate standards. HPLC analysis involved a binary gradient. Mobile phase A consisted of 100 mM sodium acetate at pH 5.5; mobile phase B consisted of 100% acetonitrile. The flow rate was set at 1.6 ml/min. The gradient consisted of 100% A from 0 to 5 min, then 85% A/15% B from 5 to 27.5 min. Fractions were mechanically collected every min for the first 10 min and then every 10 s for the duration of the run. Radioactivity of the fractions was measured with a scintillation counter. Intracellular levels of radiolabeled compounds are expressed as picomoles per milligram of protein, based on calculated percentages in the peaks from the HPLC chromatogram and total picomoles per milligram of cellular [^{3}H]antifolate. To confirm the identities of the early-eluting peaks as polyglutamate metabolites of compound **1**, samples were hydrolyzed to their parent drug forms by an overnight treatment at 32°C with a preparation of partially purified chicken pancreas conjugase in 0.5 ml of 0.1 M sodium borate, pH 7.8, containing 10 mM 2-mercaptoethanol (Matherly et al., 1985). Samples were deproteinized by boiling (5 min) then analyzed by HPLC.

In Situ GARFT Enzyme Inhibition Assay. Incorporation of [^{14}C(U)]glycine into [^{14}C]formyl GAR as an in situ measure of endogenous GARFTase activity in folate-depleted R1-11-PCFT4 cells at pH 6.8 was performed using a modification of published methods (Beardsley et al., 1989; Deng et al., 2008). For these experiments, R1-11-PCFT4 cells were seeded in 5 ml of complete folate-free RPMI 1640 medium/10% dFBS, plus 25 nM LCV in 60 mm dishes and allowed to adhere overnight. Cells were washed twice with DPBS and resuspended in 5 ml of complete folate-free RPMI 1640 medium/10% dFBS with 25 mM PIPES/25 mM HEPES, pH 6.8, and 25 nM LCV. Antifolate inhibitor or an equivalent amount of vehicle (e.g., DMSO) ("control") was added to the culture medium, and the cells were incubated for another 16 h. Cells were washed twice with DPBS and resuspended in 5 ml of complete folate-free, L-glutamine-free RPMI 1640 medium/10% dFBS plus 25 mM PIPES/25 mM HEPES, pH 6.8, and 25 nM LCV with or without 0.5 to 100 nM antifolate and azaserine (final concentration, 4 μM), and incubated for 30 min. L-Glutamine (final concentration, 2 mM) and [^{14}C]glycine (final specific activity, 0.1 mCi/l) were added, followed by incubation at 37°C for 8 h, after which time cells were washed three times with ice-cold DPBS and trypsinized. Cell pellets were suspended in 2 ml of 5% trichloroacetic acid at 0°C. Cell debris was removed by centrifugation; samples were solubilized in 0.5 N NaOH and assayed for protein contents (Lowry et al., 1951). The supernatants were ex-

tracted twice with 2 ml of ice-cold ether. The aqueous layer was passed through a 1-cm column of AG1x8 (chloride form, 100–200 mesh) (BioRad Laboratories, Hercules, CA), washed with 10 ml of 0.5 N formic acid, followed by 10 ml of 4 N formic acid, and eluted with 8 ml of 1 N HCl solution. The elutants were collected as 1-ml fractions and determined for radioactivity.

Determination of Intracellular ATP levels. For analysis of ATP levels after antifolate treatments, R1-11-PCFT4 cells were seeded in 10 ml of complete folate-free RPMI 1640 medium/10% dFBS, with 25 mM PIPES/25 mM HEPES, pH 6.8, and 25 nM LCV. After 24 h, 10 μM compound **1** or DMSO (final concentration, 0.5%) (control) was added to the culture medium. Cells were incubated for an additional 24 to 72 h, after which they were trypsinized and washed twice with ice-cold DPBS. Nucleotides were extracted and ATP levels quantitated by HPLC exactly as described previously (Kugel Desmoulin et al., 2010b).

Assessment of Apoptosis and Cell Cycle Distribution. R1-11-PCFT4 cells were treated with 10 μM compound **1** for 48 h at pH 6.8 in complete folate-free RPMI 1640 medium/10% dFBS with 25 mM PIPES/25 mM HEPES, pH 6.8, and 25 nM LCV. Cells were trypsinized, pelleted, and washed once with ice-cold DPBS. Samples were divided so that the cell cycle profile and apoptosis analysis could be performed on the same sample. The amount of apoptosis was measured by staining cells ($\sim 10^6$) with fluorescein isothiocyanate (FITC)-conjugated annexin V and propidium iodide (PI) with the apoptotic cells determined using the CELL LAB ApoScreen Annexin V-FITC Apoptosis Kit (Beckman Coulter, Fullerton, CA), as recommended by the manufacturer. Cells were analyzed for the presence of viable (annexin V^- and PI^-), early apoptotic (annexin V^+ and PI^-), and late apoptotic/necrotic (annexin V^+ and PI^+) cells by flow cytometry.

To determine compound **1** concentration-dependent effects on cell-cycle progression, R1-11-PCFT4 cells (10^6) were treated with 0, 0.5, 1, 5, and 10 μM compound **1** in complete folate-free RPMI 1640 medium/10% dFBS with 25 mM PIPES/25 mM HEPES, pH 6.8, and 25 nM LCV for 48 h at pH 6.8. Cells ($\sim 10^6$) were fixed in ethanol (at least 1 h), then stained by resuspension in 0.5 ml of DPBS containing 50 μg/ml PI and 100 μg/ml RNase type I-A (Sigma Aldrich, St. Louis, MO). The cells were analyzed by flow cytometry for determining the percentage of cells in each phase of the cell cycle.

Flow cytometry was performed at the Karmanos Cancer Institute Imaging and Cytometry Core using the BD FACSCanto II operated with BD FACSDiva software (v6.0) (BD Biosciences, San Jose, CA). In each experiment, 2×10^4 cells were assessed for apoptosis and cell cycle distribution. Data were analyzed with the FlowJo software (ver. 7.6.1; Tree Star, Inc, Ashland, OR).

In Vivo Efficacy Study of Compound 1 in HepG2 Xenografts. Cultured HepG2 human hepatoma tumor cells were implanted subcutaneously ($\sim 10^7$ cells/flank) to establish a solid tumor xenograft model in female ICR SCID mice (National Institutes of Health DCT/DTP Animal Production Program, Frederick, MD). For the efficacy study, mice were 8 weeks old on day 0 (tumor implant) with an average body weight of 17.6 g. Mice were provided food and water ad libitum. Study mice were maintained on either a folate-deficient diet (Harlan-Teklad, Madison, WI) or a folate-replete diet (autoclavable mouse breeder diet) starting 16 days before subcutaneous tumor implant to ensure serum folate levels would approximate those of humans. Folate serum levels were determined before tumor implantation and after the study with a *Lactobacillus casei* bioassay (Varela-Moreiras and Selhub, 1992). The animals were pooled and implanted bilaterally subcutaneously with 30- to 60-mg tumor fragments by a 12-gauge trocar and again pooled before unselective distribution to the various treatment and control groups. Chemotherapy was begun 4 days after tumor implantation, when the number of cells was relatively small (10^7–10^8 cells; before the established limit of palpation). Tumors were measured with a caliper two or three times weekly. Mice were sacrificed when the cumulative tumor burden reached 1500 mg. Tumor weights were estimated from two dimensional measurements [i.e., tumor mass (in milligrams) = $(ab^2)/2$, where a and b are the tumor length and width in millimeters, respectively]. For calculation of end points, both tumors on each mouse were added together, and the total mass per mouse was used. The following quantitative end points were used to assess antitumor activities: 1) T/C and $T - C$ (tumor growth delay) [where T is the median time in days required for the treatment group tumors to reach a predetermined size (e.g., 500 mg) and C is the median time in days for the control group tumors to reach the same size; tumor-free survivors are excluded from these calculations]; and 2) calculation of tumor cell kill [log10 cell kill total (gross) = $(T - C)/(3.32)(T_d)$, where $(T - C)$ is the tumor growth delay, as described above, and T_d is the tumor volume doubling time in days, estimated from the best fit straight line from a log-linear growth plot of control group tumors in exponential growth (100- to 800-mg range)]. With the exception of the xenograft model, these methods are essentially identical to those described previously (Wang et al., 2010).

Results

Expression and Function of RFC and PCFT in Human Solid Tumor and Leukemia Cell Lines. On the basis of a report of a low pH transport activity in solid tumor cell lines (Zhao et al., 2004), presumably reflecting PCFT, we turned our attention to establishing an expression profile for hPCFT compared with hRFC and FRs in a number of cell lines derived from human solid tumors and leukemias. Transcript levels for hPCFT, hRFC, and FRs α and β were measured by real-time RT-PCR and normalized to GAPDH. Our results showed significant levels of hPCFT transcripts in the majority of human solid tumor cell lines of different origins (e.g., breast, prostate, ovarian, etc.) (Fig. 2A), and uniformly low hPCFT transcript levels in human leukemias, including both ALL and acute myeloid leukemia (Supplemental Fig. 1S, C). hPCFT levels were highest in Caco-2 (colorectal adenocarcinoma), SKOV3 (ovarian carcinoma), HepG2 (hepatoma), and H69 (small cell lung cancer) cells, with appreciable hPCFT levels in numerous other tumor sublines. hRFC transcripts were detected in all solid tumor and leukemia cell lines with the exception of MDA-MB-231 breast cancer cells (Fig. 2B and Supplemental Fig. 1S, D). High levels of FRα were detected in a small subset of ovarian, cervical, and breast cancer cell lines, and low but detectable FRα levels were measured in ALL (mostly T-cell) sublines (Supplemental Fig. 1S, A and B). FR β transcripts were consistently low to undetectable in both solid tumors and leukemias, with the highest levels restricted to a small number of acute myeloid leukemia and T-cell ALL sublines (not shown).

Effects of Compound 1 on Cell Growth Inhibition and Colony Formation in HeLa and HepG2 Human Tumor Sublines. Our previous studies (Wang et al., 2010) established that the novel pyrrolo[2,3-*d*]pyrimidine thienoyl antifolate compound **1** (Fig. 1) was a potent (nanomolar) inhibitor of proliferation of a Chinese hamster ovary (CHO) subline engineered to express hPCFT in the absence of other folate transporters (RFC and FRs) and of [^{3}H]Mtx transport by hPCFT, suggesting competitive binding to the carrier (and transport by this mechanism). Conversely, the data strongly suggested that compound **1** was not transported by hRFC in a CHO subline similarly engineered to exclusively express hRFC.

To begin to establish the therapeutic potential of hPCFT as a selective approach for chemotherapy drug delivery to human solid tumors, we used isogenic HeLa sublines derived by stable

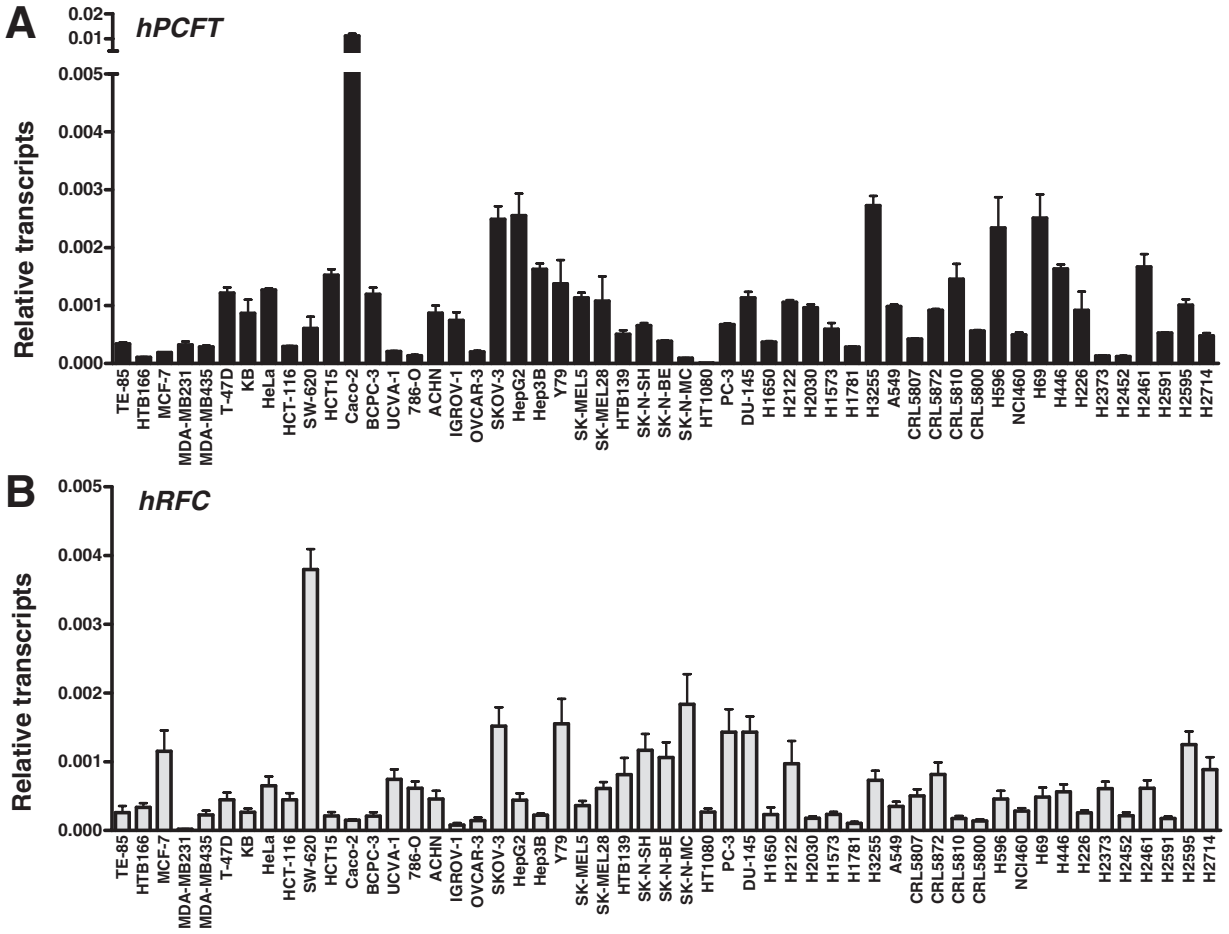

Fig. 2. PCFT and RFC expression in human solid tumor cell lines. hPCFT (top) and hRFC (bottom) transcripts were measured in 53 human solid tumor cell lines by real-time RT-PCR from total RNAs using a Roche480 Light-cycler. Transcript levels were normalized to GAPDH transcripts. Experimental details are provided under *Materials and Methods*. Results for FRα and for transporter levels in 27 human leukemia cell lines are included in Supplemental Fig. 1S, A to D. A table summarizing the characteristics of the 53 tumor and 27 leukemia cell lines is also included in Supplemental Table 1S.

transfections of hRFC- and hPCFT-null R1-11 HeLa cells, designated R1-11-PCFT4 (express physiologic levels of hPCFT in the absence of hRFC, as measured by real-time RT-PCR) and R1-11-RFC6 (engineered to express hRFC without hPCFT), (Zhao et al., 2008) (Fig. 3A). Low levels of FRα were detected in all the R1-11 sublines. As a tumor prototype, we used HepG2 cells, established from our tumor cell line screen to express significant levels of hPCFT and hRFC (Fig. 2) without FRα (expression levels for hPCFT and hRFC in HepG2 cells are compared with those for the R1-11 sublines in Fig. 3A).

We measured inhibition of cell proliferation by compound **1** and results were compared with those for Pmx. Pmx inhibited cell growth in both the R1-11-PCFT4 and R1-11-RFC6 lines with IC_{50} values (mean ± S.E.M.) of 59.3 ± 7.37 and 81.7 ± 5.49 nM, respectively (Fig. 3B), demonstrating its lack of specificity for hPCFT over hRFC despite its high PCFT substrate activity (Zhao et al., 2008; Kugel Desmoulin et al., 2010b). Conversely, compound **1** inhibited cell growth in R1-11-PCFT4 cells (IC_{50}, 99.2 ± 20.2 nM) but not R1-11-RFC6 (Fig. 3C), indicating selective hPCFT transport. In HepG2 cells, both Pmx (IC_{50}, 40.63 ± 4.52 nM) and compound **1** (IC_{50}, 227.50 ± 8.98 nM) were growth inhibitory. The decreased sensitivity to compound **1** for HepG2 cells compared with R1-11-PCFT4 cells probably reflects the presence of hRFC in HepG2 cells. Although not active for transport with compound **1**, hRFC still transports folates and elevates intracellular folate pools, resulting in decreased cytotoxic drug effects on this basis.

Proliferation assays were extended to include colony-forming assays, in which R1-11-PCFT4 cells were exposed to a range of concentrations (1–10 μM) of compound **1** (Fig. 3D) or Pmx (E) for 16, 24, or 48 h. Drug exposures were performed at pH 6.8, after which drugs were removed and colonies allowed to outgrow for 12 days. As an inhibitor of colony formation, Pmx and compound **1** showed both concentration and time dependence, although this effect was more pronounced for compound **1,** and Pmx was more active at 16 h for the lower drug concentrations. Despite the latter activity, the maximum extent of inhibition after 48 h at 10 μM drug was greater for compound **1** (95%) than for Pmx (87%).

Collectively, these results demonstrate that compound **1**, like Pmx, is cytotoxic toward cells that express hPCFT, and under acidic conditions (pH 6.8), achievable in solid tumors. Unlike Pmx, compound **1** is selectively active toward cells expressing hPCFT and is inactive toward cells expressing exclusively hRFC.

Transport Characteristics for [^{3}H]6-Substituted Pyrrolo[2,3-*d*]Pyrimidine Thienoyl Antifolate Compound 1 in HeLa R1-11-PCFT4 and HepG2 Cells. To directly measure hPCFT membrane transport of the cytotoxic antifo-

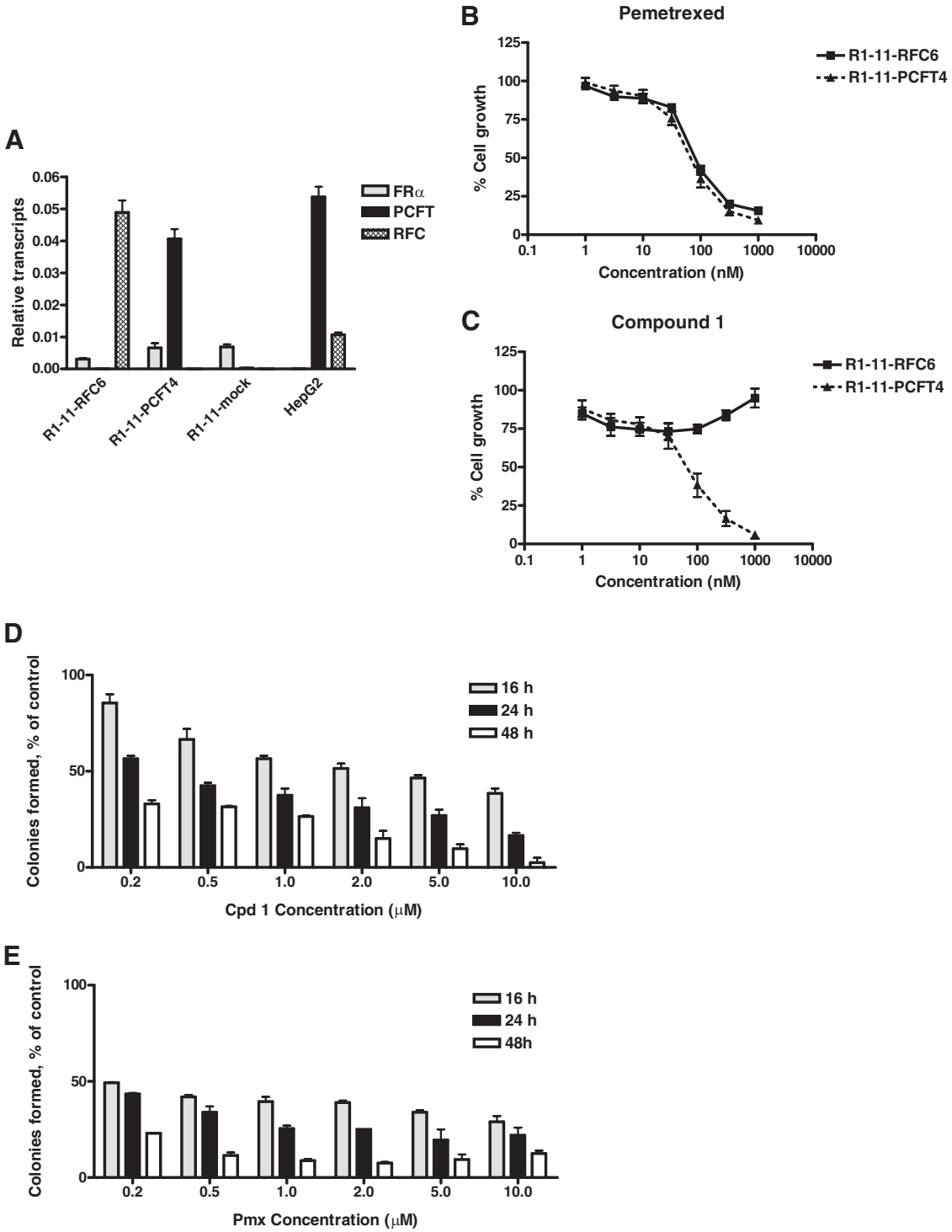

Fig. 3. Characterization of folate transporter expression and compound **1** and Pmx growth inhibition and inhibition of colony formation in R1-11 sublines and HepG2 cells. A, FRα, hPCFT and hRFC transcript levels in R1-11 sublines and HepG2 cells was measured by real-time RT-PCR. B and C, growth inhibition curves for folate-depleted R1-11-PCFT4 and -RFC6 cells treated with Pmx or compound **1** for 96 h are shown. D and E, R1-11-PCFT4 cells were plated in 60-mm dishes at a density of 500 cells per dish. After 48 h, the cells were treated at pH 6.8 in the presence or absence of different concentrations of compound **1** or Pmx from 0 to 10 μM for 16, 24, and 48 h, followed by drug washout. Plates were scored by counting visible colonies after 12 days (by staining with methylene blue) and presented as a percentage of vehicle control.

lates into HeLa R1-11-PCFT4 and HepG2 cells, we used radiolabeled compound **1** and Pmx. For R1-11-PCFT4 cells, uptake of [^{3}H]compound **1** (0.25 μM) was time- and pH-dependent with maximum drug accumulation at pH 5.5 (Fig. 4, A–C). Uptake in R1-11-PCFT4 cells exceeded that of its hPCFT-null isogenic counterpart (R1-11-mock transfectant), unequivocally establishing transport of compound **1** by hPCFT. The modest time-dependent uptake in the hPCFT-null R1-11-mock transfected subline was particularly obvious at 30 min and probably reflects the presence of low levels of FR in these cells (Fig. 3A).

We compared the uptake of [^{3}H]Pmx with that of [^{3}H]com-

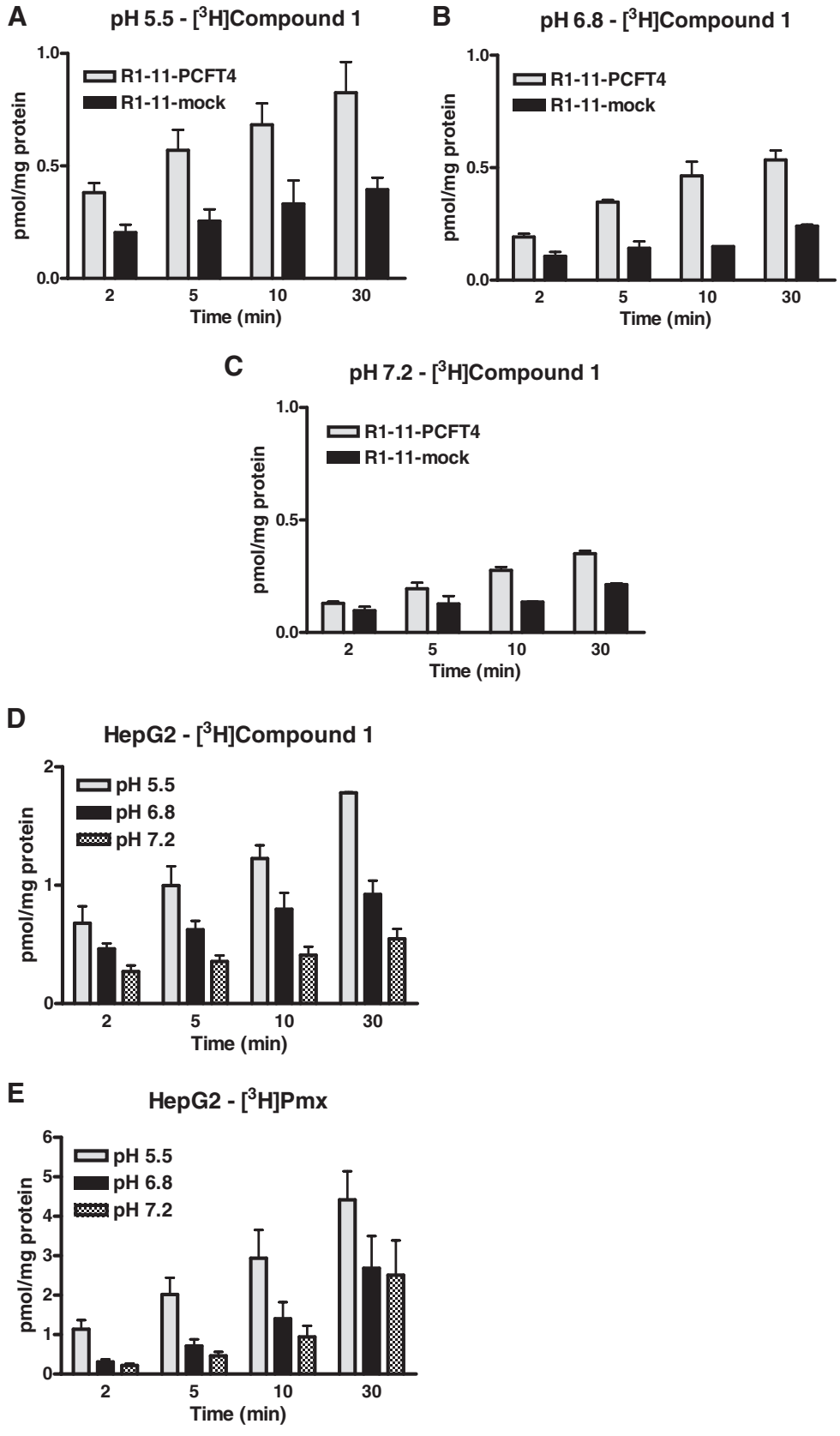

Fig. 4. pH- and time-dependent transport of compound **1** and Pmx into R1-11-PCFT4 and HepG2 cells. Direct hPCFT transport activity of compound **1** (A–D) and Pmx (E) in R1-11-PCFT4 (A–C) and HepG2 (D and E) cells was assessed by measuring uptake of 0.25 μM [^{3}H]compound **1** or [^{3}H]Pmx over 2 to 30 min at 37°C in complete folate-free RPMI 1640 medium (pH 5.5, 6.8, and 7.2), supplemented with 10% dFBS and 25 mM HEPES/25 mM PIPES. Internalized [^{3}H]compound **1** and [^{3}H]Pmx were normalized to total protein and expressed as picomoles per milligram of protein.

pound **1** in HepG2 cells (Fig. 4, D and E). For compound **1**, pH-dependent uptake in HepG2 cells showed a profile (despite the ~2-fold increased net uptake) similar to that of R1-11-PCFT4 HeLa cells. Net uptake of [^{3}H]Pmx exceeded that of [^{3}H]compound **1** in HepG2 cells by ~50 to 100% and showed a greater uptake fraction at neutral pH, most likely due to the presence of hRFC in HepG2 cells (Fig. 3A).

We measured transport kinetics over 2 min for [^{3}H]com-

TABLE 1
Kinetic constants for hPCFT

Kinetic constants for compound **1** and Pmx (K_t and V_{max}) were determined with [^{3}H]compound **1** and [^{3}H]Pmx, respectively, and calculated from Lineweaver Burk plots with R1–11-PCFT4 HeLa cells. Results are presented as mean values ± S.E. from three experiments.

Substrate and Parameter	pH 5.5	pH 6.8
Pmx		
K_t, μM	0.03 ± 0.003	4.43 ± 0.253
V_{max}, pmol · mg^{-1} · min^{-1}	1.27 ± 0.023	2.18 ± 0.317
V_{max}/K_t	42.3	0.49
Compound **1**		
K_t, μM	0.02 ± 0.013	5.91 ± 1.36
V_{max}, pmol · mg^{-1} · min^{-1}	1.76 ± 0.154	3.08 ± 0.451
V_{max}/K_t	88	0.52

pound **1** and [^{3}H]Pmx in R1-11-PCFT4 cells using a range of drug concentrations at pH 5.5 and 6.8 (Table 1). The data show nearly identical K_t values for compound **1** and Pmx at pH 5.5 and only modest (within ~40%) differences in V_{max}. Increases in both K_t (increased ~300- to 400-fold, respectively, compared with values at pH 5.5) and V_{max} values (~70% increased) were measured at pH 6.8. V_{max}/K_t ratios for compound **1** and Pmx were similar (within ~2-fold) at both pH 5.5 and pH 6.8. These results establish that for both R1-11-PCFT4 and HepG2 cells, compound **1** is an excellent substrate for hPCFT, essentially equivalent to Pmx.

Polyglutamylation of the 6-Substituted Pyrrolo[2,3-*d*]pyrimidine Thienoyl Antifolate Compound 1 in R1-11-PCFT4 and HepG2 Cells. Polyglutamylation of classic antifolates is a critical factor in drug activity, because these conjugated drug forms are retained within cells and they typically inhibit folate-dependent enzyme targets to a greater extent than their nonpolyglutamyl forms (Goldman and Matherly, 1985; Shane, 1989). To assess the extent of this metabolism for compound **1** in R1-11-PCFT4 and HepG2 cells, cells were treated with 1 μM [^{3}H]compound **1** for 16 h at pH 6.8 in the presence of adenosine (60 μM). For HepG2 cells, parallel incubations were performed with [^{3}H]Pmx [in presence of thymidine (10 μM) and adenosine]. ^{3}H-labeled metabolites were extracted and analyzed by reversed-phase HPLC (Fig. 5 shows an HPLC chromatograph for compound **1** in HepG2 cells; additional results for R1-11-PCFT4 and HepG2 cells are included in the Supplemental Fig. 2S, A and B). Up to five polyglutamyl metabolites of [^{3}H]compound **1** and [^{3}H]Pmx (PG_{2-6}) were resolved by HPLC. The identities of the peaks were confirmed by comparing elution times with those for Mtx polyglutamyl standards and by treatment with chicken pancreas conjugase which reverted the majority of the polyglutamyl metabolites to the parental drug (Supplemental Fig. 2S, C).

The distributions of the individual compound **1** and Pmx drug forms in R1-11-PCFT4 and HepG2 cells are summarized in Table 2. Although there were differences in the relative amounts of total intracellular compound **1** between the R1-11-PCFT4 and HepG2 sublines (as expected from the transport results in Fig. 4), in both cases, compound **1** was predominantly polyglutamylated (64 and 84% of the total intracellular drug, respectively). For HepG2 cells, the increased accumulation of [^{3}H]compound **1** over that of R1-11-PCFT4 cells was reflected in the polyglutamate levels. Analogous results were obtained with [^{3}H]Pmx in HepG2 cells, although the net extent of drug uptake and metabolism of [^{3}H]Pmx was elevated over that of [^{3}H]compound **1**. Collectively, these results establish that, like Pmx, compound **1** is an excellent substrate for polyglutamylation under conditions (pH 6.8) that favor its membrane transport by hPCFT.

Validation of GARFTase and De Novo Purine Nucleotide Biosynthesis As Primary Cellular Targets for Compound 1 in R1-11-PCFT4 Cells. We previously reported that the principal intracellular target of compound **1** in hPCFT-expressing CHO cells is GARFTase (Wang et al., 2010), the first folate-dependent enzyme in de novo purine nucleotide biosynthesis. To confirm this result in R1-11-PCFT4 HeLa cells under acidic conditions (pH 6.8) that favor PCFT transport, we used an in situ metabolic assay that quantifies incorporation of [^{14}C]glycine into [^{14}C]formyl GAR as a measure of GARFTase inhibition. Results were compared with those of Pmx, an established GARFTase inhibitor, along with its documented effects on thymidylate synthase (Chattopadhyay et al., 2007) and 5-amino-4-imidazolecarboxamide ribonucleotide formyltransferase (Racanelli et al., 2009) (Fig. 6). IC_{50} values for GARFTase inhibition in R1-11-PCFT4 cells by compound **1** and Pmx were 43.6 and 69.7 nM, respectively. Although the IC_{50} for GARFTase inhibition by compound **1** closely approximated the IC_{50} for growth inhibition of R1-11-PCFT4 cells (Fig. 3C), GARFTase inhibition by Pmx was incomplete up to 5 μM. Analogous results were described for Pmx with hPCFT-expressing CHO cells (R2/

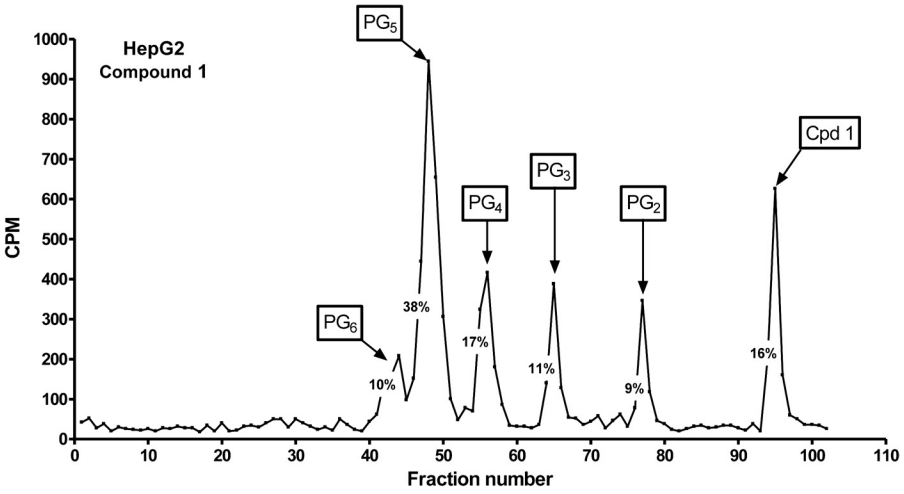

Fig. 5. HPLC analysis of polyglutamyl derivatives of compound **1** in HepG2 cells at pH 6.8. HepG2 cells were treated with 1 μM [^{3}H]compound **1** at pH 6.8 in the presence of adenosine (60 μM) for 16 h. Polyglutamates were extracted by boiling in 50 mM phosphate buffer, pH 6.0, containing 100 mM 2-mercaptoethanol and separated on a 5 μm Spherisorb C-18 ODS-2 column (4.6 × 250 mm) with a Nova-Pak 4 μm C-18 guard column. Fractions were collected, and radioactivity was measured. Percentage monoglutamate and polyglutamate drug forms were determined by chromatographic analysis, and the total intracellular radiolabeled drug was calculated in units of picomoles per milligram of protein (Table 2).

TABLE 2

Distribution of compound 1 and Pmx polyglutamates in R1–11-PCFT4 and HepG2 cells

Cells were incubated for 16 h with 1 μM [^{3}H]compound **1** or [^{3}H]Pmx. Drug accumulations and HPLC analysis of [^{3}H]polyglutamate metabolites were performed as described under *Materials and Methods*.

Metabolites	Compound **1**				Pmx HepG2	
	R1–11-PCFT4		HepG2			
	pmol/mg	%	*pmol/mg*	%	*pmol/mg*	%
Total drug	5.8		12.8		41.6	
PG_6	0		1.3	10	7.4	18
PG_5	1.4	24	4.9	38	10.3	25
PG_4	0.78	14	2.2	17	4.1	10
PG_3	1.0	18	1.5	12	5.8	14
PG_2	0.48	8	1.2	9	3.7	9
PG_1[a]	2.1	36	2.1	16	8.8	21

[a] Parent (unmetabolized) drug.

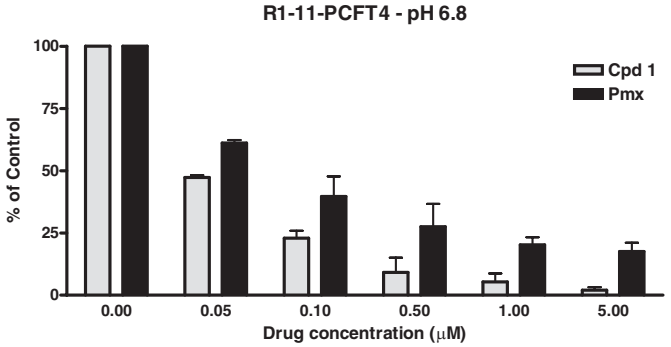

Fig. 6. In situ GARFTase inhibition by compound **1** and Pmx in R1-11-PCFT4 cells. GARFTase activity and inhibition were evaluated in situ with R1-11-PCFT4 cells. R1-11-PCFT4 cells were treated with drug for 16 h at pH 6.8 in complete folate-free RPMI 1640 medium supplemented with 10% dFBS, and 25 mM HEPES and 25 mM PIPES before incubating in the presence of 4 μM azaserine for 30 min, followed by [^{14}C]glycine and L-glutamine treatment. After 8 h, radioactive metabolites were extracted and fractionated on 1-cm columns of AG1x8(Cl^-) and the fractions were collected and radioactivity was measured. Accumulation of [^{14}C]formyl GAR was calculated as a percent of vehicle control over a range of antifolate concentrations.

hPCFT4) (Kugel Desmoulin et al., 2010b) and with CCRF-CEM cells by Racanelli et al. (2009).

To confirm that potent inhibition of GARFTase in R1-11-PCFT4 cells by compound **1** also results in decreased ATP pools, we measured intracellular ATP levels in cells treated with 10 μM compound **1** for 16, 24 and 48 h under acidic conditions (pH 6.8) analogous to those used for our clonogenicity studies (Fig. 3D). Compound **1** caused a time-dependent decrease in cellular ATP levels, such that treatment for 48 h led to an 88% decrease in ATP pools (Fig. 7A). These results demonstrate that hPCFT-delivery of compound **1** is an efficient mode of drug uptake that effects a potent inhibition of GARFTase and ATP depletion in R1-11-PCFT4 cells.

Effect of Compound 1 on Cell Cycle Progression and Apoptosis Induction in R1-11-PCFT4 Cells. To determine the impact of GARFTase inhibition and ATP depletion on cell-cycle progression, we treated R1-11-PCFT4 cells with compound **1** (10 μM) for 48 h at pH 6.8, along with a vehicle control. Cells were fixed, stained with PI, and analyzed for cell cycle distribution by flow cytometry. Treatment with 10 μM compound **1** caused an accumulation of cells in S phase such that 38.9% of cells were in S phase, compared with 16.8% of the control (Fig. 7B; Supplemental Fig. 3S). When a range of concentrations (0.5, 1, 5, and 10 μM) of compound **1** were tested for their abilities to induce S-phase accumulation, we found that maximal arrest was achieved at 1 μM.

Because treatment with compound **1** (10 μM, 48 h at pH 6.8) causes loss of clonogenicity in R1-11-PCFT4 cells (Fig. 3D) and a modest increase in the sub-G_1 fraction (Fig. 7B), we were interested in measuring apoptosis under these same conditions using annexin V/PI staining. Results were compared with those for R1-11-PCFT4 cells treated with etoposide (5 μM) and with a no-drug control. Whereas etoposide strongly induced apoptosis (12.2% early apoptotic and 22.3% late apoptotic/necrotic) compared with the negative controls (2.9 and 10.3%, respectively), compound **1** was less apoptotic (8.4 and 15.7%, respectively) (Fig. 7C). These results are consistent with previous reports that GARFTase inhibitors are distinctly cytotoxic, yet modestly apoptotic (Smith et al., 1993; Deng et al., 2008).

In Vivo Efficacy Study of Compound 1 against HepG2 Xenografts. As proof of concept that in vivo antitumor efficacy can result from tumor targeting of compound **1** via its transport by hPCFT, an in vivo efficacy trial was performed with 8-week-old female ICR SCID mice implanted with subcutaneous HepG2 tumors that express hPCFT and hRFC but not FRα (Fig. 3A). Mice were maintained ad libitum on folate-deficient or standard folate-replete diets. Serum folate concentrations were measured in mice after 14 days on the folate-deficient diet by an *L. casei* bioassay; the value was 90.2 nM (median) [range, 79.2–120.7 nM (n = 3)]. This value slightly exceeds serum folate levels (31 and 35 nM, respectively) reported previously in humans (Ganji and Kafai, 2009). With the standard diet, by comparison, serum folate was 715.2 nM (median) [range, 652.8–742.8 nM (n = 3)]. For the trial, control and drug treatment groups were nonselectively randomized (five mice per group); compound **1** was administered intravenously on a schedule of every 4 days for three treatments (180 mg/kg per injection) on days 4, 8, and 12 after implantation (total dose 540 mg/kg). Results were compared with those for paclitaxel (Taxol; every 2 days for six treatments, 7.5 mg/kg per injection). Mice were weighed daily and tumors were measured 2 to 3 times per week. For the mice maintained on the folate-deficient diet, appreciable antitumor activity was recorded with compound **1** (T/C of 0% on day 21; $T - C$ = 13 days; 1.4 gross log kill) (Fig. 8), exceeding that for paclitaxel (T/C = 16%; 0.8 gross log kill). Antitumor drug efficacy for **1** was completely abolished (99% T/C) for the standard folate-replete diet. The treatment regimen was well tolerated with dose-limiting symptoms manifesting as reversible body weight loss for mice maintained on the folate-deficient diet. Results for the in vivo efficacy experiment shown in Fig. 8 are summarized in Supplemental Table 3S.

The results of the in vivo efficacy trial demonstrate potent antitumor activity for compound **1** toward subcutaneously engrafted HepG2 tumors associated with significant transport by hPCFT and a lack of membrane transport by hRFC.

Discussion

In this study, we significantly expand upon previous reports (Zhao and Goldman, 2007; Kugel Desmoulin et al., 2010b) suggesting that PCFT may be therapeutically exploitable for treating solid tumors. We found that hPCFT, like hRFC, was widely and highly expressed in an extensive

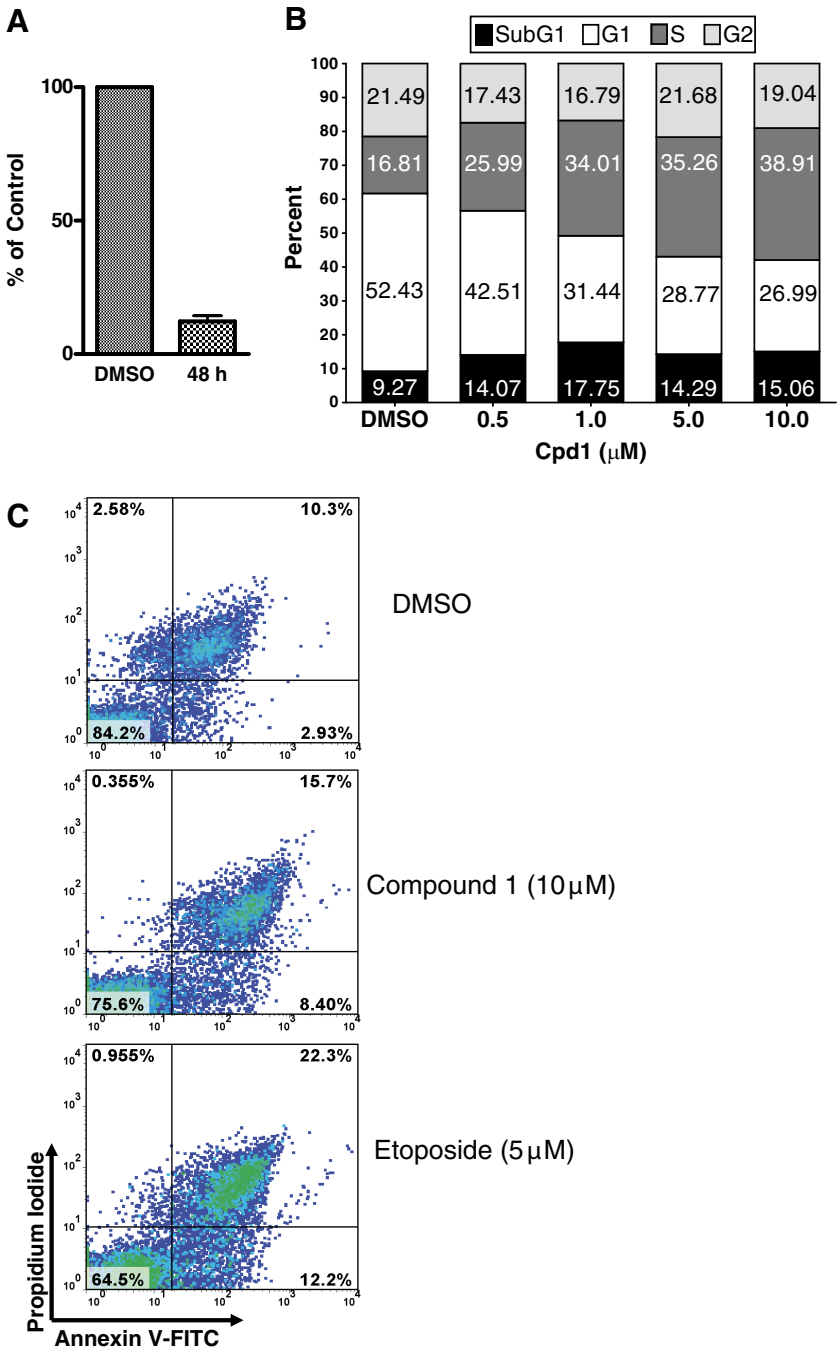

Fig. 7. Compound 1 treatment depletes ATP levels and induces an S-phase cell accumulation, accompanied by a modest level of apoptosis in R1-11-PCFT4 cells. A, for analysis of ATP levels, cells were treated with 10 μM compound **1** or left untreated (DMSO) for 48 h at pH 6.8. Nucleotides were extracted, and ATP pools were determined by a modification of the HPLC method of Huang et al. (Huang et al., 2003), as described previously (Kugel Desmoulin et al., 2010b). Details are provided under *Materials and Methods*. B, the percentages of cells in each phase of the cell cycle (G_1, S, and G_2), including those in the sub-G_1 fraction, were determined in R1-11-PCFT4 cells treated with a range of concentrations of compound **1** for 48 h by measuring the cellular DNA content with PI staining and flow cytometry. Representative cell cycle profiles are shown in the Supplement (Fig. 3S). C, pseudo-color dot plots show the flow cytometric analysis of cells stained with annexin V-FITC and PI. The percentages of viable cells (annexin V−/PI−), early apoptotic cells (annexin V+/PI−), and late apoptotic/necrotic cells (annexin V+/PI+) are noted. As a positive control, cells were treated with 5 μM etoposide for 48 h at pH 6.8 to induce apoptosis.

panel of human solid tumor cell lines but not in human leukemias. Another group showed that low pH transport activity of Mtx was prominent in human tumor cell lines (Zhao et al., 2004), in direct support of the findings reported herein. Twelve of the human sublines were included in both studies, and for these, there was reasonable correlation between hPCFT and hRFC transcript levels and transport activity at pH 5.5 and 7.4, respectively. We further show that the novel 6-substituted pyrrolo[2,3-*d*]pyrimidine thienoyl antifolate compound **1** can be selectively transported by hPCFT in a pH- and time-dependent manner. The tumor models employed, R1-11-PCFT4 HeLa and HepG2 cells, express similar levels of hPCFT, although they differ in the presence of hRFC and FRα.

The premise behind our drug discovery efforts, exemplified by compound **1**, is that membrane transport of cytotoxic antifolates is a critical determinant of antitumor drug selectivity. Compound **1** is not transported by the ubiquitously expressed RFC (Wang et al., 2010). This is particularly important because drugs such as compound **1** that target FRα and/or PCFT, yet are not substrates for RFC, have the potential to selectively target tumor cells and decrease toxicity to normal tissues. This is a substantial advantage over chemotherapy drugs currently in use; indeed, pursuing the development of these novel antifolates could yield a new class of clinically relevant antitumor agents. Our previous work used engineered CHO models, as well as KB (nasopharyngeal) and IGROV1 (ovarian) human tumor cells that express FRα

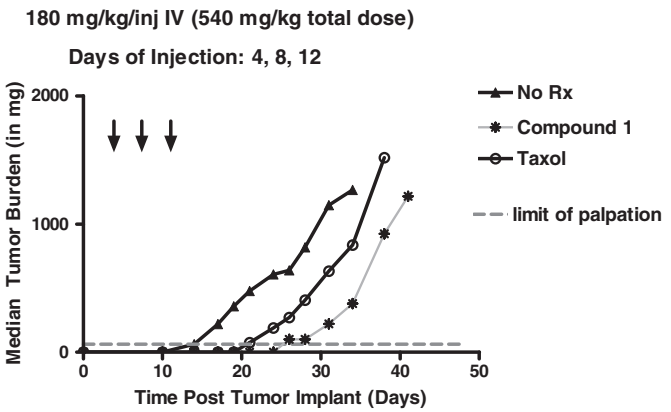

Fig. 8. In vivo efficacy trial of compound **1** in HepG2 xenografts. Female ICR SCID mice were maintained on a folate-deficient diet ad libitum. Human HepG2 tumors were implanted bilaterally and mice were nonselectively randomized into five mice per group. Compound **1** [dissolved in 5% ethanol (v/v), 1% Tween 80 (v/v), and 0.5% $NaHCO_3$] was administered on a schedule of every 4 days for three intravenous treatments on days 4, 8, and 12 (indicated with arrows) at 180 mg/kg/injection. Paclitaxel (dissolved in water) was administered on a schedule of every 2 days for six treatments (7.5 mg/kg injection) beginning on day 4. Mice were observed and weighed daily; tumors were measured twice per week. For the mice maintained on the folate-deficient diet and treated with compound **1**, appreciable antitumor activity was recorded ($T/C = 0\%$; $T - C =$ 13 days; 1.4 gross log kill). Data are shown for the median tumor burdens and are summarized in Supplemental Table 3S.

and/or hPCFT to deliver cytotoxic antifolates, including compound **1,** that are not substrates for hRFC (Deng et al., 2008, 2009; Wang et al., 2010). The present report significantly expands upon this concept by demonstrating exclusive transport of compound **1** by hPCFT into human tumor cell lines at pH values characterizing the tumor microenvironment. For R1-11-PCFT4 and HepG2 cells, after its internalization at pH 6.8, compound **1** was extensively polyglutamylated, such that the predominant metabolite was the pentaglutamate form (compound **1** conjugated to 4 glutamate residues). Moreover, compound **1** potently inhibited GARFTase, leading to R1-11-PCFT4 HeLa cell death in vitro and HepG2 tumor growth delay in vivo.

Expression of hPCFT transcripts and protein in normal human tissues is more restrictive than for hRFC, high hPCFT levels being observed in the liver, kidney, and small intestine and very low levels in the bone marrow and colon (Kugel Desmoulin et al., 2010a). This pattern of PCFT transcripts was generally observed in mouse tissues (Qiu et al., 2007). Our finding that hPCFT transcripts are low in human bone marrow (Kugel Desmoulin et al., 2010a) is particularly significant and suggests that hPCFT-targeted therapeutics may be less marrow toxic than antifolates presently in clinical use.

The microenvironments for most normal tissues probably exhibit a neutral pH (Martin and Jain, 1994), such that even if PCFT is present, the electrochemical proton gradient is reduced, leading to less accumulation of PCFT substrates such as compound **1**. Conversely, RFC would exhibit a far greater activity under these conditions. This, when combined with the greater capacity of RFC to transport reduced folates across the cell membrane compared with PCFT (Zhao et al., 2008), would result in elevated levels of cellular folates in normal tissues. The increased availability of reduced folates would result in competition with internalized antifolates for polyglutamylation and/or for binding to intracellular drug targets (e.g., GARFTase), thus protecting normal cells from drug cytotoxicity. Likewise, for PCFT-targeted agents in solid tumors, if sufficient RFC were present, enough transport of folates might occur even at slightly acidic pH values to decrease drug efficacy on this basis. This implies that the ratio of PCFT to RFC in tumors is critical to antitumor activities of PCFT-selective cytotoxic antifolates and that Mtx-resistant tumors that have substantially lost RFC function may be exquisitely sensitive to the effects of PCFT-selective drugs such as compound **1**. Thus, for compound **1** and related agents, tumor selectivity is not only reliant upon differential PCFT levels between normal tissues and solid tumors but is also affected by interstitial pH and activity of RFC.

Another consideration involves the purine salvage pathway. Methylthioadenosine phosphorylase (MTAP) is an enzyme that releases adenine and 5-deoxy-5-(methylthio)ribose-1-phosphate from methylthioadenosine formed during polyamine biosynthesis (Illei et al., 2003). Adenine is used in purine salvage, and 5-deoxy-5-(methylthio)ribose-1-phosphate is subsequently recycled to methionine. Whereas MTAP has been reported to be abundantly expressed in normal tissues, in many solid tumors, the MTAP gene is codeleted with CDKN2A (encodes p16INK4A) (Illei et al., 2003). Thus, many solid tumors are deficient in purine salvage and functional purine salvage in normal tissues would theoretically protect cells from cell death caused by GARFTase inhibition, increasing tumor cell selectivity for agents such as compound **1** (Hori et al., 1996).

It is interesting that under nearly the same conditions, the IC_{50} for GARFTase inhibition in R1-11-PCFT4 cells by the in situ GARFTase assay is virtually identical to the IC_{50} for inhibition of cell proliferation. This result differs somewhat from our previous finding with an analogous 6-substituted pyrrolo[2,3-*d*]pyrimidine benozyl antifolate in CHO cells for which the IC_{50} for GARFTase inhibition was substantially lower, suggesting that sustained GARFTase inhibition was necessary to manifest as cytotoxicity (Kugel Desmoulin et al., 2010b). This quantitative difference may reflect differences in the size of purine pools between the human and hamster sublines such that R1-11-PCFT4 HeLa cells would be more sensitive to the inhibition of GARFTase. Of course, other factors could also contribute. For instance, differences in drug polyglutamylation and polyglutamate turnover could result in disparate potencies for sustained GARFTase inhibition in different cell lines.

Finally, our studies with compound **1** assess the impact of GARFTase inhibition on ATP levels and the mechanism(s) of tumor cell death. Treatment of R1-11-PCFT4 cells with compound **1** substantially reduced ATP levels and caused S-phase accumulation. Apoptosis resulting from compound **1** was reduced compared with etoposide. This could (at least in part) reflect the requirement of ATP for apoptosis, because ATP levels must be maintained above a minimal level for apoptosis induction (Tsujimoto, 1997).

In conclusion, our in vitro studies suggest the feasibility of using hPCFT and the acidic tumor microenvironment to selectively deliver a novel PCFT-targeted antifolate to human solid tumors. Our in vivo results with HepG2 tumor cells that express only hPCFT and hRFC provide compelling proof-of-principle validation and rationale for developing

drugs whose transport by PCFT, but not RFC, allows for GARFTase inhibition.

Acknowledgments

We thank Dr. I. David Goldman for the generous gift of the R1-11 HeLa cell line series (R1-11-mock, R1-11-RFC6, and R1-11-PCFT4). We thank Kelly Haagenson for editorial assistance in preparing the manuscript.

Authorship Contributions

Participated in research design: Kugel Desmoulin, Wang, Hales, Polin, Hou, Gangjee, and Matherly.

Conducted experiments: Kugel Desmoulin, Wang, Hales, Polin, White, Kushner, Stout, Hou, and Cherian.

Performed data analysis: Kugel Desmoulin, Wang, Hales, Polin, Stout, Hou, Gangjee, and Matherly.

Wrote or contributed to the writing of the manuscript: Kugel Desmoulin, Wang, Hales, Polin, Gangjee, and Matherly.

References

Beardsley GP, Moroson BA, Taylor EC, and Moran RG (1989) A new folate antimetabolite, 5,10-dideaza-5,6,7,8-tetrahydrofolate is a potent inhibitor of de novo purine synthesis. *J Biol Chem* **264:**328–333.

Chattopadhyay S, Moran RG, and Goldman ID (2007) Pemetrexed: biochemical and cellular pharmacology, mechanisms, and clinical applications. *Mol Cancer Ther* **6:**404–417.

Deng Y, Wang Y, Cherian C, Hou Z, Buck SA, Matherly LH, and Gangjee A (2008) Synthesis and discovery of high affinity folate receptor-specific glycinamide ribonucleotide formyltransferase inhibitors with antitumor activity. *J Med Chem* **51:**5052–5063.

Deng Y, Zhou X, Kugel Desmoulin S, Wu J, Cherian C, Hou Z, Matherly LH, and Gangjee A (2009) Synthesis and biological activity of a novel series of 6-substituted thieno[2,3-d]pyrimidine antifolate inhibitors of purine biosynthesis with selectivity for high affinity folate receptors over the reduced folate carrier and proton-coupled folate transporter for cellular entry. *J Med Chem* **52:**2940–2951.

Elnakat H and Ratnam M (2004) Distribution, functionality and gene regulation of folate receptor isoforms: implications in targeted therapy. *Adv Drug Deliv Rev* **56:**1067–1084.

Fais S, De Milito A, You H, and Qin W (2007) Targeting vacuolar H+-ATPases as a new strategy against cancer. *Cancer Res* **67:**10627–10630.

Farber S and Diamond LK (1948) Temporary remissions in acute leukemia in children produced by folic acid antagonist, 4-aminopteroyl-glutamic acid. *N Engl J Med* **238:**787–793.

Ganji V and Kafai MR (2009) Demographic, lifestyle, and health characteristics and serum B vitamin status are determinants of plasma total homocysteine concentration in the post-folic acid fortification period, 1999–2004. *J Nutr* **139:**345–352.

Gibbs DD, Theti DS, Wood N, Green M, Raynaud F, Valenti M, Forster MD, Mitchell F, Bavetsias V, Henderson E, et al. (2005) BGC 945, a novel tumor-selective thymidylate synthase inhibitor targeted to alpha-folate receptor-overexpressing tumors. *Cancer Res* **65:**11721–11728.

Goldman ID and Matherly LH (1985) The cellular pharmacology of methotrexate. *Pharmacol Ther* **28:**77–102.

Helmlinger G, Yuan F, Dellian M, and Jain RK (1997) Interstitial pH and pO2 gradients in solid tumors in vivo: high-resolution measurements reveal a lack of correlation. *Nat Med* **3:**177–182.

Hilgenbrink AR and Low PS (2005) Folate receptor-mediated drug targeting: from therapeutics to diagnostics. *J Pharm Sci* **94:**2135–2146.

Hori H, Tran P, Carrera CJ, Hori Y, Rosenbach MD, Carson DA, and Nobori T (1996) Methylthioadenosine phosphorylase cDNA transfection alters sensitivity to depletion of purine and methionine in A549 lung cancer cells. *Cancer Res* **56:**5653–5658.

Huang D, Zhang Y, and Chen X (2003) Analysis of intracellular nucleoside triphosphate levels in normal and tumor cell lines by high-performance liquid chromatography. *J Chromatogr B Analyt Technol Biomed Life Sci* **784:**101–109.

Illei PB, Rusch VW, Zakowski MF, and Ladanyi M (2003) Homozygous deletion of CDKN2A and codeletion of the methylthioadenosine phosphorylase gene in the majority of pleural mesotheliomas. *Clin Cancer Res* **9:**2108–2113.

Kugel Desmoulin S, Wang Y, Tait L, Hou Z, Cherian C, Gangjee A, and Matherly LH (2010a) Expression profiling of the major folate facilitative transporters in human tumors and normal tissues, in *Proceedings of the Annual Meeting of the American Association for Cancer Research*; 2010 Apr 17–21; Washington DC. pp 1103, Abstract 4546. American Association for Cancer Research, Philadelphia.

Kugel Desmoulin S, Wang Y, Wu J, Stout M, Hou Z, Fulterer A, Chang MH, Romero MF, Cherian C, Gangjee A, and Matherly LH (2010b) Targeting the proton-coupled folate transporter for selective delivery of 6-substituted pyrrolo[2,3-d]pyrimidine antifolate inhibitors of de novo purine biosynthesis in the chemotherapy of solid tumors. *Mol Pharmacol* **78:**577–587.

Lowry OH, Rosebrough NJ, Farr AL, and Randall RJ (1951) Protein measurement with the Folin phenol reagent. *J Biol Chem* **193:**265–275.

Martin GR and Jain RK (1994) Noninvasive measurement of interstitial pH profiles in normal and neoplastic tissue using fluorescence ratio imaging microscopy. *Cancer Res* **54:**5670–5674.

Matherly LH, Hou Z, and Deng Y (2007) Human reduced folate carrier: translation of basic biology to cancer etiology and therapy. *Cancer Metastasis Rev* **26:**111–128.

Matherly LH, Voss MK, Anderson LA, Fry DW, and Goldman ID (1985) Enhanced polyglutamylation of aminopterin relative to methotrexate in the Ehrlich ascites tumor cell in vitro. *Cancer Res* **45:**1073–1078.

Mendelsohn LG, Worzalla JF, and Walling JM (1999) Preclinical and clinical evaluation of the glycinamide ribonucleotide formyltransferase inhibitors lometrexol and LY309887, in *Anticancer Drug Development Guide: Antifolate Drugs in Cancer Therapy* (Jackman AL ed) pp 261–280, Humana Press, Inc., Totowa, NJ.

Monahan BP and Allegra CJ (2006) Antifolates, in *Cancer Chemotherapy and Biotherapy* (Chabner BA, Longo DL ed) pp 91–124, Lippincott Williams & Wilkins, Philadelphia.

Nakai Y, Inoue K, Abe N, Hatakeyama M, Ohta KY, Otagiri M, Hayashi Y, and Yuasa H (2007) Functional characterization of human proton-coupled folate transporter/heme carrier protein 1 heterologously expressed in mammalian cells as a folate transporter. *J Pharmacol Exp Ther* **322:**469–476.

Qiu A, Jansen M, Sakaris A, Min SH, Chattopadhyay S, Tsai E, Sandoval C, Zhao R, Akabas MH, and Goldman ID (2006) Identification of an intestinal folate transporter and the molecular basis for hereditary folate malabsorption. *Cell* **127:**917–928.

Qiu A, Min SH, Jansen M, Malhotra U, Tsai E, Cabelof DC, Matherly LH, Zhao R, Akabas MH, and Goldman ID (2007) Rodent intestinal folate transporters (SLC46A1): secondary structure, functional properties, and response to dietary folate restriction. *Am J Physiol Cell Physiol* **293:**C1669–C1678.

Racanelli AC, Rothbart SB, Heyer CL, and Moran RG (2009) Therapeutics by cytotoxic metabolite accumulation: pemetrexed causes ZMP accumulation, AMPK activation, and mammalian target of rapamycin inhibition. *Cancer Res* **69:**5467–5474.

Raghunand N, Altbach MI, van Sluis R, Baggett B, Taylor CW, Bhujwalla ZM, and Gillies RJ (1999) Plasmalemmal pH-gradients in drug-sensitive and drug-resistant MCF-7 human breast carcinoma xenografts measured by 31P magnetic resonance spectroscopy. *Biochem Pharmacol* **57:**309–312.

Salazar MD and Ratnam M (2007) The folate receptor: what does it promise in tissue-targeted therapeutics? *Cancer Metastasis Rev* **26:**141–152.

Shane B (1989) Folylpolyglutamate synthesis and role in the regulation of one-carbon metabolism. *Vitam Horm* **45:**263–335.

Smith SG, Lehman NL, and Moran RG (1993) Cytotoxicity of antifolate inhibitors of thymidylate and purine synthesis to WiDr colonic carcinoma cells. *Cancer Res* **53:**5697–5706.

Tsujimoto Y (1997) Apoptosis and necrosis: intracellular ATP level as a determinant for cell death modes. *Cell Death Differ* **4:**429–434.

Varela-Moreiras G and Selhub J (1992) Long-term folate deficiency alters folate content and distribution differentially in rat tissues. *J Nutr* **122:**986–991.

Wang L, Cherian C, Desmoulin SK, Polin L, Deng Y, Wu J, Hou Z, White K, Kushner J, Matherly LH, et al. (2010) Synthesis and antitumor activity of a novel series of 6-substituted pyrrolo[2,3-d]pyrimidine thienoyl antifolate inhibitors of purine biosynthesis with selectivity for high affinity folate receptors and the proton-coupled folate transporter over the reduced folate carrier for cellular entry. *J Med Chem* **53:**1306–1318.

Wike-Hooley JL, Haveman J, and Reinhold HS (1984) The relevance of tumour pH to the treatment of malignant disease. *Radiother Oncol* **2:**343–366.

Zhao R, Gao F, Hanscom M, and Goldman ID (2004) A prominent low-pH methotrexate transport activity in human solid tumors: contribution to the preservation of methotrexate pharmacologic activity in HeLa cells lacking the reduced folate carrier. *Clin Cancer Res* **10:**718–727.

Zhao R and Goldman ID (2003) Resistance to antifolates. *Oncogene* 22(47):7431–7457.

Zhao R and Goldman ID (2007) The molecular identity and characterization of a proton-coupled folate transporter—PCFT; biological ramifications and impact on the activity of pemetrexed. *Cancer Metastasis Rev* **26:**129–139.

Zhao R, Matherly LH, and Goldman ID (2009) Membrane transporters and folate homeostasis: intestinal absorption and transport into systemic compartments and tissues. *Expert Rev Mol Med* **11:**e4.

Zhao R, Qiu A, Tsai E, Jansen M, Akabas MH, and Goldman ID (2008) The proton-coupled folate transporter: impact on pemetrexed transport and on antifolates activities compared with the reduced folate carrier. *Mol Pharmacol* **74:**854–862.

Address correspondence to: Dr. Larry H. Matherly, Developmental Therapeutics Program, Barbara Ann Karmanos Cancer Institute, 110 E. Warren Ave, Detroit, MI 48201. E-mail: matherly@kci.wayne.edu